Emission features of femtosecond laser ablated carbon plasma in ambient helium

K. F. Al-Shboul, S. S. Harilal, and A. Hassanein
Center for Materials Under Extreme Environment, School of Nuclear Engineering, Purdue University, West Lafayette, Indiana 47907, USA

We investigated the optical emission features of plasmas produced by 800 nm, 40 fs ultrafast laser pulses on a carbon target in the presence of ambient helium or nitrogen gases at varied pressures. Fast photography employing intensified charge coupled device, optical emission spectroscopy, and temporally spatially resolved optical time of flight emission spectroscopy were used as diagnostic tools. Spatio-temporal contours of excited neutral, ionic, as well as molecular carbon species in the plume were obtained using time of flight emission spectroscopy. These contours provided detailed account of molecular species evolution and expansion dynamics and indicate that three-body recombination is a major mechanism for carbon dimers generation in ultrafast laser ablation plumes in the presence of ambient gas. A systematic comparison of the emission features from ns and fs laser ablation carbon plumes as well as their expansion in ambient helium is also given. C_2 vibrational temperatures were estimated during carbon plasma expansion with lower values in ambient helium compared to nitrogen and showed decreasing values with respect to space and ambient gas pressure. © 2013 AIP Publishing LLC. [http://dx.doi.org/10.1063/1.4803096]

I. INTRODUCTION

The interaction of laser ablated plumes with an ambient gas is of great interest for diverse applications, e.g., pulsed laser deposition (PLD), laser-ablation inductively coupled-plasma mass-spectrometry (LA-ICP-MS), nanoparticles and aerosol formation, laser induced breakdown spectroscopy (LIBS), etc. Further interesting applications of laser ablation (LA) plumes are evolving since the advent of low-cost and compact ultrafast lasers in recent years. Ultrafast LA is found to have more advantages compared to traditional nanosecond LA in many of these applications including less droplets in PLD,[1] reduced elemental fractionation in LA-ICP-MS,[2] precise micromachining,[3] reduced continuum emission in LIBS, etc.[4,5] The use of ultrashort lasers, i.e., fs lasers, has a reduced thermal effect on the ablated material compared to ns LA and an ablation depth with improved precision can be obtained.[6,7] These special characteristics of fs LA have initiated new research paths for more detailed understanding of ultrafast laser-material interactions, plasma excited species expansion dynamics, and mechanisms of material removal.[8] A detailed comparison of ns and fs laser ablations is described elsewhere.[9,10] Regardless of laser pulse duration (fs-ns), laser produced-plasmas (LPPs) are highly transient in both space and time, so studying plasma expansion dynamics and emitting species' kinetic properties is essential for most applications.[11]

Laser produced carbon plasmas have many applications,[12–14] such as diamond-like carbon (DLC) deposition,[15] nanostructures production including carbon nanotubes,[14] nanowires, graphene,[16] etc. The kinetic properties of LPP species and their ionization degree strongly affect the deposited films quality.[17] DLC films generated during ultrafast PLD at room temperature showed high chemical inertness and resistance along with strong optical transparency.[18] Moreover, nanoparticles generation by ultrafast LA was also observed during plasma late time evolution.[19] It is known that carbon dimers, i.e., C_2, play prominent role in carbon clusters and nanoparticles formation.[14,20] Our recent studies using ns LA showed that C_2 existence in vacuum is limited to short distances and earliest times, while the presence of ambient gas enhanced C_2 formation in the extended region of the laser plumes generated by three-body recombination.[21] We have also observed oscillations in C_2 emission intensity as the monochromatic images showed that C_2 distribution is not uniform and it is more localized at various points in carbon ns LPP plumes.[22] Laser parameters, such as wavelength,[23] pulse width,[10] and focal spot size[24] are important factors that critically change the dynamics of the emitting species in laser ablation plumes.[25] While a great effort has been expended in recent years for studying the dynamics of carbon ns laser ablated plumes,[21,22,25–27] experiments for investigating spatial and temporal evolutions of the emitting species during femtosecond LA are still limited.

In this article, we report on the expansion dynamics of carbon ultrafast laser produced plasma in the presence of ambient helium or nitrogen gases. We investigated the evolution history of carbon plasma as well as various species in the plume *viz.* excited C_2 molecules, carbon neutrals, and ions using fast imaging and optical emission spectroscopy (OES). Temporal-spatial contours generated by optical time-of-flight emission spectroscopy (OTOF-ES) techniques were used to make a systematic comparison among the evolutions of various carbon excited species during the fs LPP expansion. In addition, comparisons of the current results with those obtained from ns LPPs are also discussed.

II. EXPERIMENTAL

In this work, carbon plasmas are produced using either 800 nm, 40 fs, 10 Hz pulses from Ti:Sapphire laser or 1064 nm, 6 ns, 10 Hz pulses from an Nd:YAG laser. Figure 1 shows the schematic of the experimental setup used for fs LA. The fs laser system consists of a mode-locked Ti-Sapphire oscillator (Synergy 20, Femtolasers Inc.), which gives 75 MHz, ~800 nm pulses with 40 nm bandwidth. The amplifier system (Amplitude Technology Inc.) consists of a stretcher, regenerative amplifier, multi-pass amplifier, and a compressor providing 10 Hz, 40 fs p-polarized pulses at ~10 mJ. The energy of the fs laser system is varied using a combination of half-wave plate and polarizer positioned prior to the compressor grating. The carbon target (graphite, Alfa-Aesar), in the form of disc, was mounted inside a stainless steel vacuum chamber pumped down to a base pressure of about 10^{-6} Torr. The target was continuously translated inside the chamber using an x-y-z translator to provide a fresh surface for each laser shot. The chamber was filled with helium or nitrogen gas at specific pressure level (0.4, 1, or 5 Torr). The laser beam was focused normal to the target surface, using a planar convex lens, making a 100 μm spot size with ~87 J cm^{-2} fluence. For synchronizing the timing of all the electronics, we used a combination of programmable timing generator (PTG) and photodiode for monitoring the onset of each laser shot. Using two appropriate collimating and focusing lenses, the emission from the LPP was imaged onto the slit of a 0.5 m spectrograph (Acton SP-2500i) that is equipped with three dispersing gratings (150, 600, and 1800 g/mm). By mounting these lenses on micrometer stages, this setup was used to collect and image the emission from the plasma on the spectrograph slit at specific distances form the target surface with high precision one-to-one correspondence. For light detection, the spectrograph is equipped with two detectors, i.e., an intensified charged coupled device (ICCD, Princeton Instruments, Pi-MAX) and a photomultiplier tube (PMT, Hamamatsu R928). A diverting mirror is used for changing the dispersed light path to the ICCD or PMT detectors. The ICCD was also used for obtaining 2D time-resolved images of the 3D expanding plasma plume. For obtaining monochromatic images of C_2 emission, a narrow band-pass filter (BPF) was used for discriminating and filtering (0-0) C_2 Swan band transition at 516 nm.

III. RESULTS AND DISCUSSION

A. Time-resolved plume imaging

2D images of the carbon LPP plumes, with a spatial resolution better than 60 μm, were recorded at different times after the impact of the ultrafast laser pulse. Typical recorded time-resolved plume images are shown in Figure 2 at different helium gas pressures (0.4 and 1 Torr). For comparison, plume imaging obtained during ns LA of carbon at 1 Torr ambient helium[21] is also given in Figure 2.

The fs LPP images show plume expansion up to ~1 cm in both lateral and axial directions. Despite the fact that ultrafast LA has much greater laser power density at the target compared to ns LA, the images show that the plumes produced by ultrafast lasers have less intensity and are more uniform and forward centric. In comparison, ns carbon plumes showed spherical-like expansion with internal structures represented by intensity oscillations in both lateral and axial directions.[21,22] The lower emission intensity of ultrafast LA plumes can be understood by considering the lower energy used in the present studies and lack of laser-plasma interaction and hence reheating. During ultrafast laser ablation, the material ejection happens in time frame of approximately ten's to hundreds of picoseconds after laser illumination and fs laser pulse-ejected material interaction does not occur[28] while during ns LA, the ejected material is heated via inverse bremsstrahlung and/or photoionization processes.

To study the effects of the ambient gas nature on fs laser carbon plasma emission features, plume images were
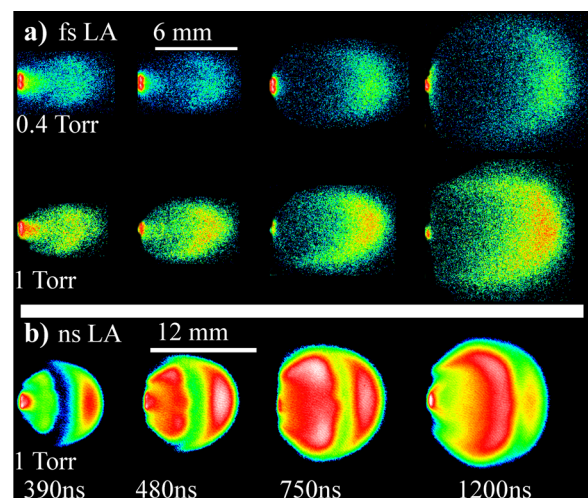
FIG. 2. Time-resolved ICCD images of carbon LPP (a) using ~87 Jcm^{-2}, 40 fs LA in 0.4, or 1 Torr ambient helium pressures and (b) using ~50 J cm^{-2}, 6 ns LA in 1 Torr ambient helium.[21] Each image is a spectrally integrated in the visible range (350-800 nm) and obtained from a single laser shot. To show the intensity oscillations (in ns LA plumes) and for better clarity, all images are normalized to the maximum intensity of that image.
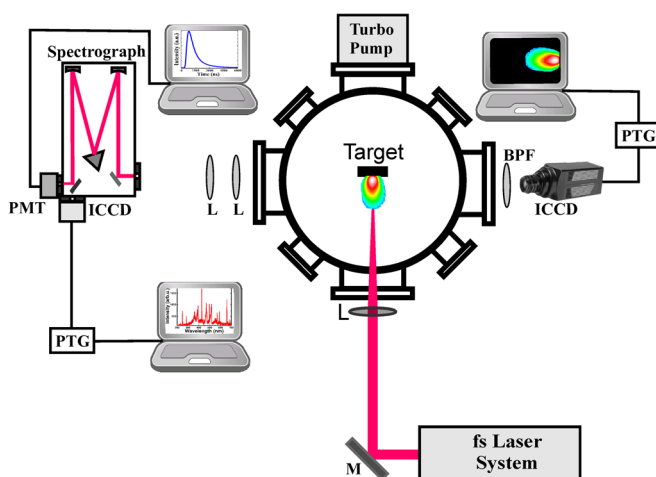
FIG. 1. Schematic of the experimental setup used. (L, lens; M, mirror; PMT, photomultiplier tube; PTG, programmable timing generator; BPF, band pass filter; and ICCD, intensified charge-coupled device).

recorded when the carbon plume expanded into ambient He or N_2 gases at similar pressure (5 Torr) and shown in Figure 3.

Although the plasma had more emission using nitrogen gas, however, this emission was limited to about ∼5 mm away from the target surface. In contrast, plasma emission was evident up to ∼8 mm when expanding into helium gas. C_2 emission features are also completely different in ambient N_2 comparing to ambient He. In agreement with previous studies,[21,30,31] the fast monochromatic ICCD images show that C_2 emission is more intense but stalled and restricted to close zone of the target surface (up to ∼4 mm) in ambient N_2, while C_2 weaker emission with more expansion was evident up to ∼7 mm from the target surface in the case of ambient helium. The stronger plasma confinement due to much heavier N_2 molecules promotes the excitation processes closer to target surface causing stronger emission with less plasma expansion.[30,31] These results were also confirmed by OES shown in Figure 7, where spectra of carbon fs plasmas are captured in both ambient gases at varied distances.

The ICCD images are also useful for obtaining better insights of plasma expansion dynamics by generating position-time (R-t) plots given in Figure 4. The estimated fs LPP plume velocities obtained from these R-t plots, by taking the slope of their linear fittings at early times (<1000 ns), are found to be about 8×10^5 cm/s, 7×10^5 cm/s, and 5.6×10^5 cm/s at 0.4, 1, and 5 Torr ambient helium, respectively.

As can be seen from Figure 4, the plume expansion is well described by the drag force model (solid lines).[32] This model is used to describe LPPs expansion at moderate ambient gas pressures[31] and it assumes plume deceleration due to drag forces by the surrounding gas, where this deceleration is proportional to the plume travelling velocity. According to the drag model,[33] the plasma expansion distance (R) at a specific time (t) is given by,
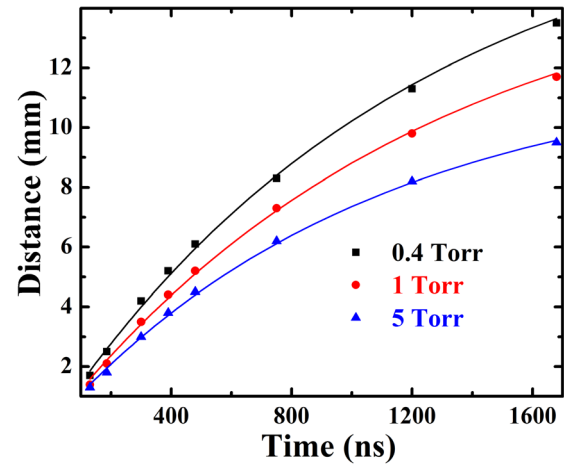
FIG. 4. Position–time (R-t) plots of the carbon ultrafast laser ablation plume front position at 0.4, 1, and 5 Torr ambient helium pressures and measured from the visible spectrally integrated ICCD images. The symbols represent experimental data points and solid lines represent the drag expansion model.

$$R = R_f(1 - e^{-\beta t}), \qquad (1)$$

where R_f is the plume stopping distance and β is the damping coefficient. Using this model, the estimated plume stopping distances were found to be 18, 16, and 12 mm for 0.4, 1, and 5 Torr ambient helium pressures, respectively. The adiabatic expansion model described by Dyer et al.[34] was also used for obtaining plume length estimates in this work. Dyer's model assumes that the ejected species pushes the ambient gas particles until they come to equilibrium. Using this model, the estimated values of plume length at 0.4, 1, and 5 Torr ambient helium pressures were 19, 16, and 11 mm, respectively. These values agree very well with the experimental values obtained from the ICCD images and the drag model as well. It is interesting to mention that in our recent work with carbon ns LPPs,[22] the plasma images showed two expansion fronts traveling with different velocities. In those experiments,[22] the faster component followed the shock wave model[35] while the expansion of the slower moving species was well described by the drag model.

B. Optical emission spectroscopy

Typical emission spectra (solid lines) obtained from carbon plasma generated using ultrafast laser pulses with ∼87 J cm^{-2} fluence per pulse is given in Figure 5. For comparison, the spectra (short dot lines) recorded during ns LA with ∼50 J cm^{-2} fluence per pulse is also given. All Spectra were recorded at a distance of 1 mm from the target surface with 2.5 μs integration time when the plume was expanding in the presence of 0.4, 1, or 5 Torr ambient helium pressures using a single laser shot.

During our time-resolved OES measurements, not shown here, we observed emissions from various excited carbon species at times much longer than their corresponding lifetimes.[36] Thus, there must be mechanisms taking place during the plasma evolution responsible for such excitations like ions-electrons collisional recombination, where the observed species is with one lower positive charge.[17,36,37] As shown in Figure 5, the continuum emission was small
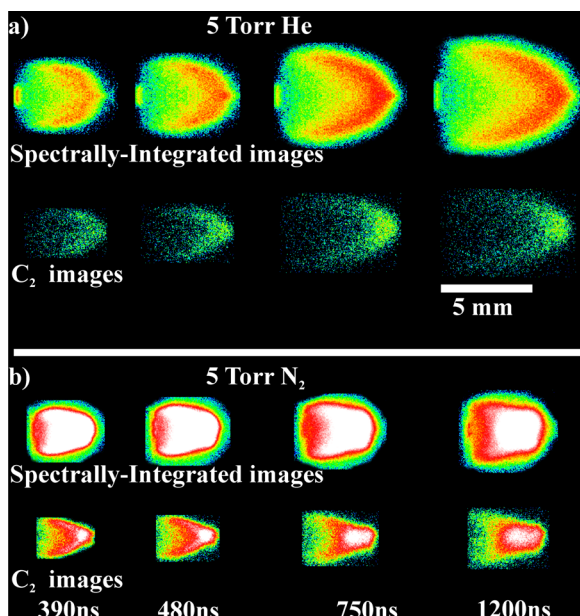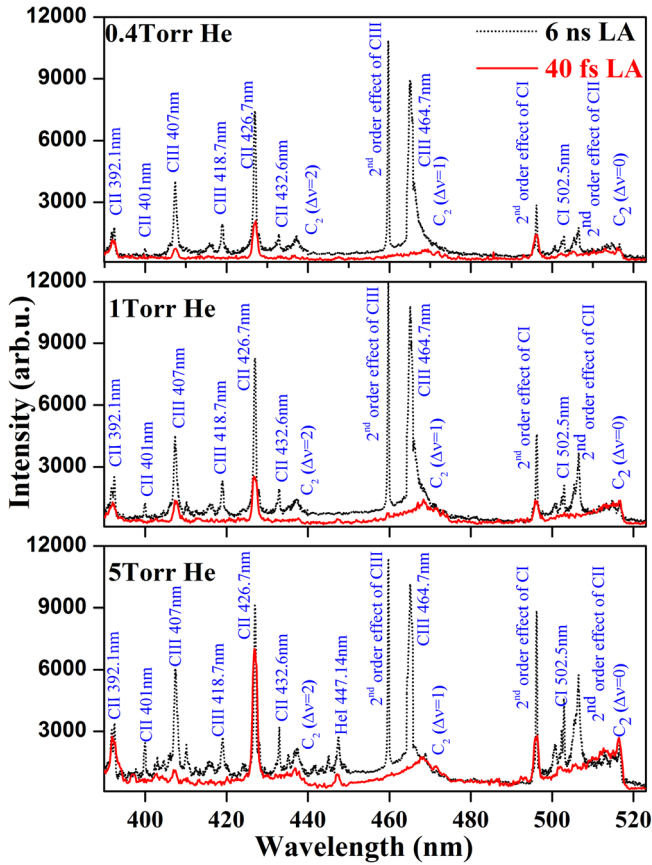

FIG. 3. Time-resolved ICCD images of carbon LPP using fs LA (a) in 5 Torr ambient helium or (b) in 5 Torr ambient nitrogen.[29] The spectrally integrated and C_2 monochromatic images are each normalized to a unified maximum value separately. Each image is obtained from a single laser shot.

FIG. 5. Spectra emitted from carbon plasma generated by $\sim$87 J cm^{-2}, fs or $\sim$50 J cm^{-2}, ns LA at varied helium pressures and at 1 mm from target surface. These spectra were obtained using the 150 g/mm grating of the spectrograph. An integration time of 2.5 μs and 30 μm spectrograph slit width was used.

compared to the recognized lines and both spectra contain emission from electronically excited C_2 radicals emitting mainly within the Swan band system corresponding to transitions between the $d^3\Pi_g$ and $a^3\Pi_u$ electronic states.[38,39] Helium gas was inserted into the chamber to enhance the emission from the plasma plume in general and carbon dimers in particular, which is extremely weak in vacuum. C_2 formation implies different processes taking place in the plume during the plasma expansion especially at plasma-gas interfacing zones.[21,22,29] The presence of background gas during the plasma expansion confines the plasma plume and enhances efficient electron impact excitation and plasma three-body recombination making the plasma more emitting. In addition, introducing background gas is necessary during cluster production or PLD for plasma cooling, controlling the plume expansion dynamics, and slowing down the energetic particles.[40–42] The spectra show strong emission from carbon lower-charged ions (especially from ns LPP), neutrals, and dimers (C_2). The spectrum emitted by ns LA is more intense and dominated by C^+ and C^{2+} lines due to higher number of photons per laser pulse and laser-plasma heating, which does not occur during fs LA.

Compared to ns LA, ultrafast LA plume mostly provides emission from neutrals, carbon dimers, along with a few singly charged ion lines. Regardless of laser excitation pulse width, the increase in ambient gas pressure leads to emission

enhancement for all species in the plasma plume. The intensities used for ultrafast laser ablation in the present experiments are larger than 10^{15} W/cm^2, which is significantly above the laser ablation threshold. At these high laser intensities, the laser ablation process is mainly contributed by thermal vaporization.[43,44] Thermal vaporization from the target produces mostly neutral species at temperatures close to the vaporization point that can be expected to emit in the visible region. The formation of C_2 could be due to three-body recombination and further spatio-temporal emission analysis is necessary for confirmation and is shown in Sec. III C.

For C_2 vibrational temperature estimation during carbon fs LA, Swan bands' emission corresponding to different vibrational transitions ($\Delta\nu = -1, 0, 1$, and 2) between the $d^3\Pi_g$ and $a^3\Pi_u$ electronic states[38,39] were captured using the 600 g/mm grating of the spectrograph at different (He or N$_2$) gas pressures and at varied distances from target surface. Figure 6 shows different Swan bands' emission of the recorded spectra at a distance of 1 mm from the target using 2 μs integration time when the plume expands through helium or nitrogen at a similar pressure level (1 Torr).

As it is evident form Figure 6, carbon fs LPP emits C_2 profoundly and the Swan bands' can be easily identified. The
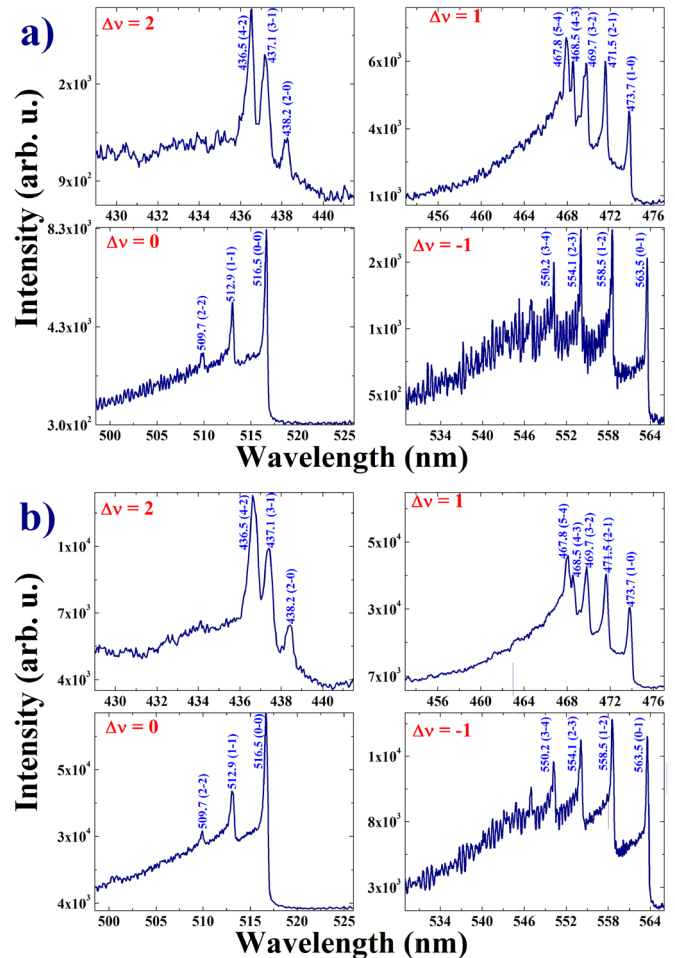

FIG. 6. ($\Delta\nu = 0, -1, 1$, and 2) C_2 Swan bands' transitions emitted form carbon fs LA plasma at 1 mm from target surface and in 1 Torr pressure of (a) helium or (b) nitrogen gases. These spectra were captured using the 600 g/mm grating with 100 μm spectrograph slit width and 2 μs integration time with respect to onset of plasma formation.

emission is more intense using ambient nitrogen as the intensity was about one order of magnitude higher compared to C_2 emission in ambient helium. Figure 7 gives the recorded spectra from fs laser carbon plasma propagating through either ambient helium or nitrogen at a pressure of 5 Torr and varied distances form target surface.

In agreement with the monochromatic C_2 ICCD images shown in Figure 3, the spectra show that inserting nitrogen gas to the ablation chamber revealed more intense C_2 emission but limited to closer distance from the target surface and there is almost no C_2 emission noticed at 5 mm from target surface. In contrast, C_2 emission was less intense but present beyond 5 mm away from the target surface when ambient helium gas was used. In the region close to the target surface, typically plume species expand with higher velocities[29] with minimal chance of collision with ambient gas specie. However, the addition of nitrogen at moderate pressures cause plasma confinement leading to enhanced collisions and recombination. Considering the heavier mass of ambient nitrogen, at similar pressure levels, more confinement can be expected when the plume expanded into nitrogen compared to ambient He.

Swan bands' emission spectra, with high resolution, were used to calculate the C_2 vibrational temperature using the summation rule of the vibrations intensities of different bands. The sums of the band strengths of all bands with the same upper (ν) or lower (ν') states are proportional to the number of molecules in the respective states. For plasma in local thermodynamic equilibrium (LTE), intensities of various vibrational levels will be related to each other according to the Boltzmann distribution[45,46]

$$ln\left(\sum_{\nu'}(\lambda^4 I_{\nu\nu'})\right) = C_1 - G(\nu)\frac{hc}{k_B T_{vib}}, \qquad (2)$$

where T_{vib} is the vibrational temperature, k_B is the Boltzmann constant, h is the Planck's constant, c is the velocity of light, λ is the corresponding emission wavelength, C_1 is a constant, and $G(v)$ is the term value corresponding to the vibrational level in the upper electronic state and can be estimated using the following relation:[45,47]

$$G(\nu) = \frac{E_{vib}}{hc} = \omega_e\left(\nu+\frac{1}{2}\right) - \omega_e x_e\left(\nu+\frac{1}{2}\right)^2 + \omega_e y_e\left(\nu+\frac{1}{2}\right)^3 + \omega_e z_e\left(\nu+\frac{1}{2}\right)^4, \qquad (3)$$

where E_{vib} represents the molecule's vibrational energy levels, and ω_e, x_e, y_e, z_e are molecular constants. The C_2 vibrational temperature was estimated by plotting the sums of the band-head strengths of vv' progressions for each upper state against the $G(v)$ term where the slope provides a direct estimation of the vibrational temperature. Figure 8 shows the variation of the vibrational temperature at various gas
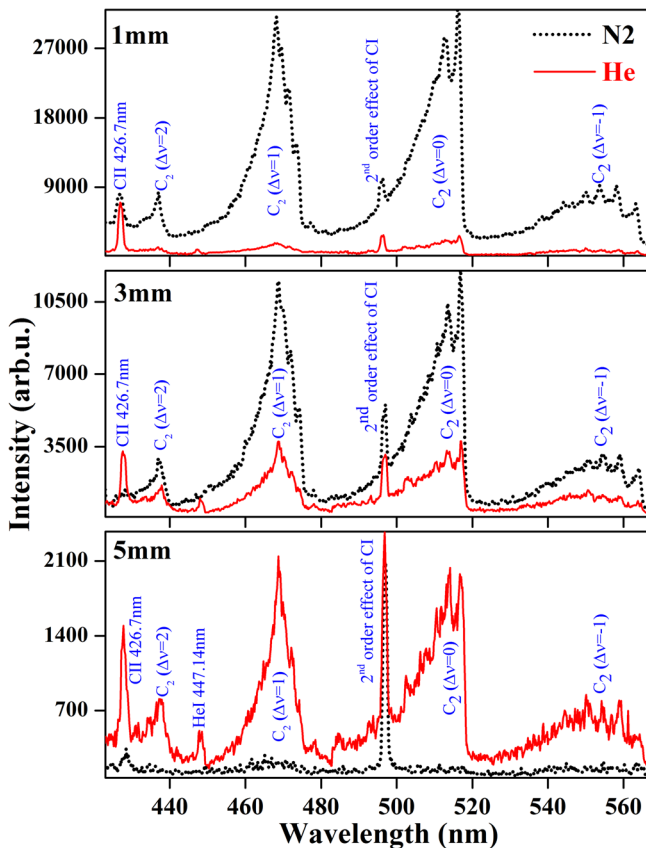

FIG. 7. Spectra emitted from carbon fs LA plasma generated in either ambient N_2 or He at similar pressure (5 Torr) and at varied distances from target surface. These spectra were captured using the 150 g/mm grating with 30 μm spectrograph slit width and 2.5 μs integration time with respect to onset of plasma formation.
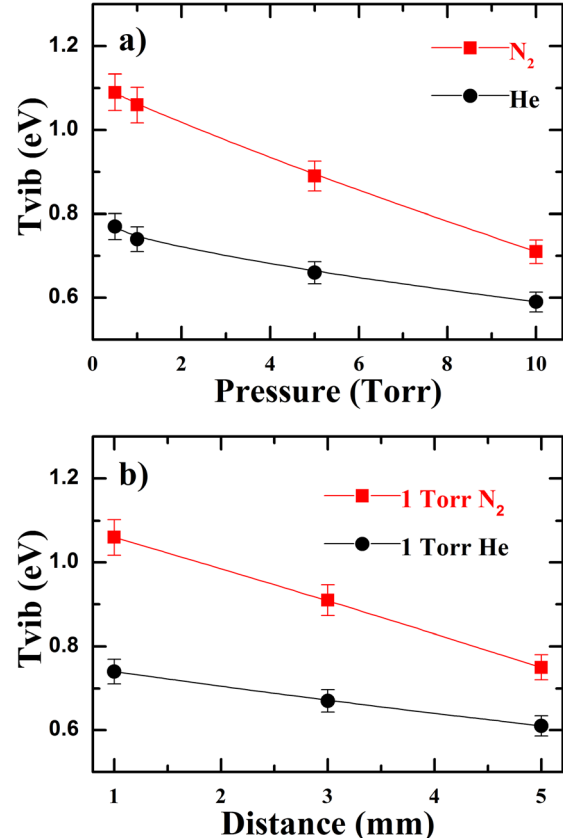

FIG. 8. Estimated C_2 vibrational temperatures of carbon plasma generated by carbon ultrafast LA at (a) at 1 mm from target surface and varied helium or nitrogen gas pressures and (b) varied distances from target surface in ambient nitrogen or helium gas at constant pressure level (1 Torr).

(helium or nitrogen) pressures and distances from the target surface.

Regardless of the ambient gas used, the vibrational temperature was found to decrease with distance from target surface. In addition, raising ambient gas pressure leads to rapid cooling of the plasma where a portion of plasma expansion energy is transferred to the ambient gas and C_2 vibrational temperature was found to be lower when the plasma propagates through ambient helium gas. This is due to high helium thermal conductivity ($0.151\,W\,m^{-1}K^{-1}$ at 1 atm and 300 K) compared to the much lower one of nitrogen ($0.026\,W$ $m^{-1}K^{-1}$ at 1 atm and 300 K).[48,49] So plasma hot electrons and excited species can be cooled down more efficiently and faster in helium gas. This is consistent with previous studies where it has been shown that the thermodynamic properties in the plasma strongly change with the molecular weight and the adiabatic exponent of ambient gas.[50] In addition, the lower mass of helium compared to nitrogen helps to increase thermal energy transfer. The plasma electron temperature decay rate due to elastic collisions is given as the following:[51,52]

$$Q = \frac{2m_e}{M}\sigma n\sqrt{\frac{8kT_e}{\pi m_e}}, \tag{4}$$

where n and M are the density and mass of ambient gas atoms, σ is the elastic scattering cross section, T_e, m_e are electron temperature and density, respectively. This shows that the electron energy transfer by elastic collisions and, hence, cooling is inversely proportional to ambient gas atomic mass and explains the lower C_2 vibrational temperatures estimations in helium gas compared to ambient nitrogen.[48–52]

C. Optical time-of-flight emission spectroscopy

Along with fast imaging and OES of ultrafast LA of carbon plasma, we also studied space-resolved temporal features of various excited (neutral and ionic) carbon species and C_2 emitting zones in the plume using OTOF-ES. OTOF-ES measurements are capable of providing time-resolved profiles with high temporal resolution (as low as 1 ns; PMT rise time) and are also useful in generating distance-time contours for certain species in the plume with high spectral purity. Typical temporal profiles of excited C_2 emission [(0-0) transition at 516.5 nm], generated by ultrafast LA of carbon at various helium pressures obtained at 4 mm from the target surface, are given in Figure 9.

Figure 9 shows that C_2 has a single-peak structure in its temporal profile preceded by a small prompt peak due to fast electron excited ambient plasma.[53] A shifted Maxwell–Boltzmann (SMB) distribution was applied to fit the time-of-flight (TOF) profile of C_2 species for a better understanding of its kinetic properties. This SMB fit is given as the following:[54]

$$f(\nu) = A\nu^3 \exp\left(-\frac{m(\nu - \nu_\circ)^2}{2kT}\right), \tag{5}$$

where A is a constant for normalization, ν is the species velocity, $\nu_\circ$ is the stream velocity, T is the species temperature,
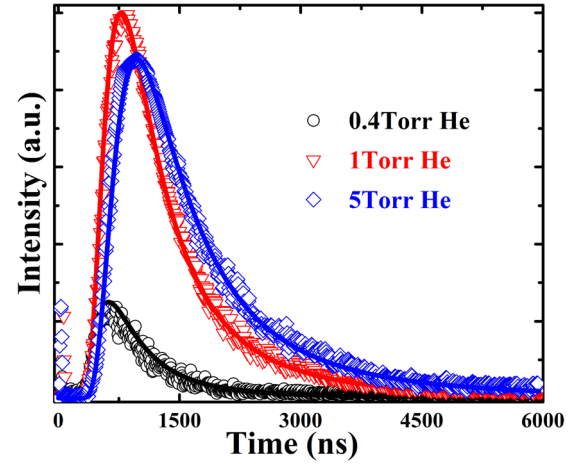

FIG. 9. Typical OTOF-ES profiles for excited C_2 species [(0-0) transition at 516.5 nm] recorded at 4 mm from the target surface, generated during ultrafast laser ablation of carbon at varied helium pressures, are given. The C_2 peaks are fitted with shifted Maxwell–Boltzmann distribution, (solid lines), using $T = 0.78\,eV$, 0.61 eV, and 0.52 eV for 0.4, 1, and 5 Torr helium pressures, respectively.

and m is the species mass. The solid lines in Figure 9 show the SMB distribution fits with estimated temperatures of $\sim$0.78 eV, 0.61 eV, and 0.52 eV for 0.4, 1, and 5 Torr helium pressures, respectively. The OTOF-ES profiles of C_2 species at different ambient helium pressures were used to generate space-time contours. These contours represent an excellent way for analyzing and studying unique emission evolution of certain species by simultaneously characterizing the emission in time and space resolved manner. Figure 10 shows C_2 optical emission spatial-temporal contours at different helium pressures.

Previous studies of carbon ns LPP experiments showed that the formation of C_2 is due to several mechanisms including recombination, dissociation of higher carbon clusters, and ejection directly from the target surface.[15,22,26,55] Because of these different C_2 formation mechanisms, two emission zones traveling with different velocities were observed during our previous carbon ns LPP studies.[21] These two zones were explained due to carbon ions recombination contributing to the faster component while carbon neutrals recombination and clusters dissociation[26] were found to be responsible for the slow moving emitting zone.[21] C_2 emission shown in Figure 10 produced by carbon ultrafast LA consists of more uniform emission distribution compared to those emission features from ns LPP;[21] meaning that there is one dominant mechanism behind C_2 formation in ultrafast carbon LPP. The estimated expansion velocities of C_2 species from these contours are: 4.7×10^5, 3.6×10^5, and 3.1×10^5 cm/s at 0.4, 1, and 5 Torr helium pressures, respectively. These velocities are less than the measured values from the time-resolved spectrally integrated ICCD plume imaging. This is not surprising considering that the plume front is mainly composed of faster ions and neutrals, while most of C_2 dimers are formed inside the plume.[17,56] Figure 10 shows that the spatial and temporal extension of C_2 emission is enhanced when the pressure is increased from 0.4 Torr to 1 Torr due to enhanced ambient gas-plasma interaction and increased recombination. However, the C_2
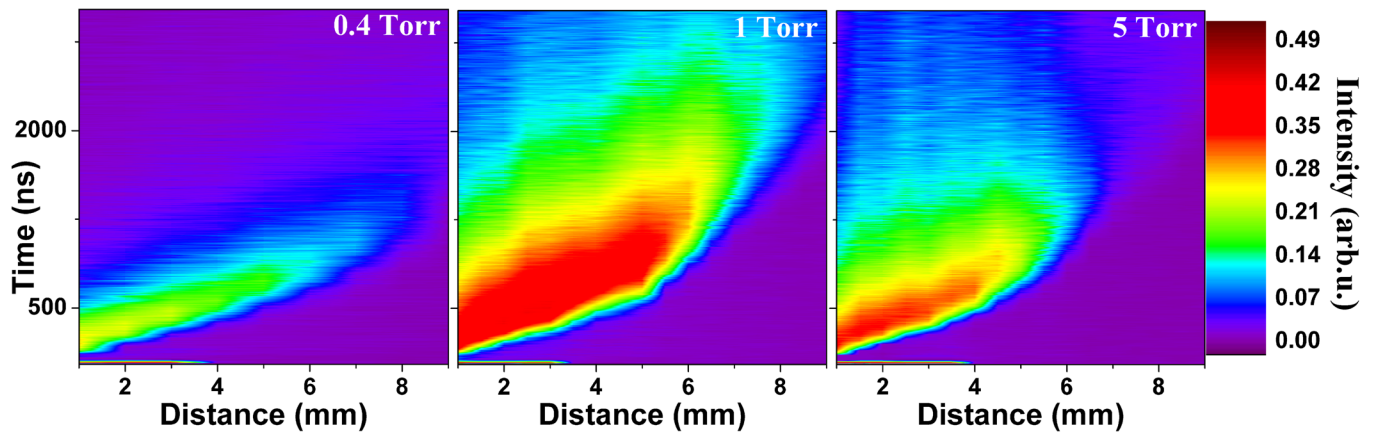
FIG. 10. Space-time contours for C_2 ($\lambda = 516.5$ nm) emission from carbon fs LPP expanding at 0.4, 1, and 5 Torr helium pressures, respectively.

emission zone is more confined when the pressure is increased from 1 Torr to 5 Torr. Similar observation on background gas pressure confinement effects on molecular emission was also previously reported.[15,57] To get more details that help understanding the nature of the formation mechanisms taking place during ultrafast carbon LPP expansion, temporal profiles of excited carbon species were recorded. Neutral carbon at 247.8 nm ($3s;\ ^1P^\circ \rightarrow 2p^2;\ ^1S$) and singly ionized carbon at 426.7 nm ($4f;\ ^2F^\circ \rightarrow 3\,d;\ ^2D$) emission profiles were obtained at different helium pressures and their corresponding space-time contours were generated. A typical TOF profile for neutral C emission generated by ultrafast LA of carbon at 0.4 Torr helium is given in Figure 11 with SMB fitting.

As it is evident from Figure 11, neutral carbon temporal profiles consist of double peak structure, where one peak travels faster than the other does. Similar double peak structure was evident for singly ionized carbon, while a single peak distribution was observed for C_2. The double peak structure for C I at 247.8 nm, given in Figure 11, is also fitted with SMB distribution (solid lines) with corresponding temperatures using T = 0.74 and 0.44 eV for the faster and slower peaks, respectively. Such double peak structures were previously reported by several groups when the expanding plume interacts with ambient gas and explained due to various formation mechanisms for the same species in the plume.[58,59] Figure 12 gives the spatial-temporal contours obtained from OTOF-ES profiles for C and C^+ at various helium ambient pressures. It shows that C and C^+ have double-peak temporal profiles. Moreover, the contours indicate that changing the helium pressure level from 0.4 to 5 Torr improves C and C^+ emission intensities. The contours also show that C_2 and C emissions in ambient helium can be related to each other taking into consideration their different propagation velocities. To make the temporal expansion dynamics of both species easier to observe, Figure 13 shows R-t plots for C_2 and C (slower peak) species obtained from their corresponding OTOF-ES profiles.

Both species expansion is decelerated with increasing ambient helium pressure. However, Figure 13 indicates that at certain helium pressure, C emission intensity peaks are always preceding C_2 emission intensity peaks with faster

propagation velocities. This is expected; taking into account that molecular C_2 is heavier than atomic C. The results obtained from the ICCD images, OES measurements, and spatio-temporal contour plots of C_2 along with excited neutral and ionic species cast better insights into their formation mechanisms in the plume expanding through ambient gas that improves the presence of excited C_2 both at latter times as well as in the extended regions due to three-body recombination.[60]

IV. SUMMARY AND CONCLUSIONS

We studied the emission dynamics of femtosecond laser produced carbon plumes in the presence of ambient helium or nitrogen gases at different pressure levels. The diagnostic tools used were ICCD fast imaging, OES, and space-resolved optical time-of-flight emission spectroscopy (OTOF-ES). A comparison is made between the plumes generated by ns and fs lasers even though the power densities differed by several orders. The time-resolved ICCD images showed that plume expansion is more uniform and forward centric for plasma generated during fs LA while plume oscillations are seen in the spherical-like expansion for ns LA.
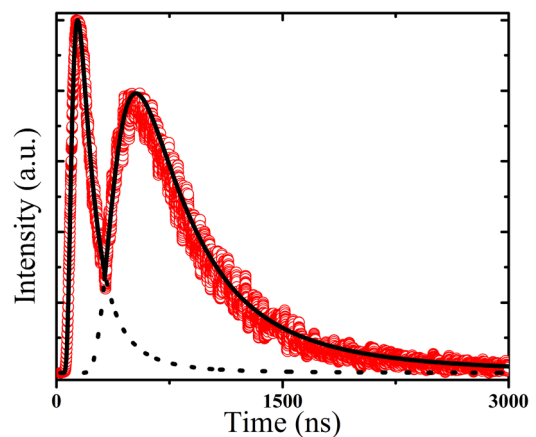

FIG. 11. Typical OTOF-ES for neutral C species ($\lambda = 247.8$ nm) recorded at 7 mm from the target surface at 0.4 Torr helium. The circles represent the data points. The C peaks are fitted with SMB distribution, (solid lines), using T = 0.74 and 0.44 eV for the faster and slower peaks, respectively, and dotted lines represent single SMB fittings.
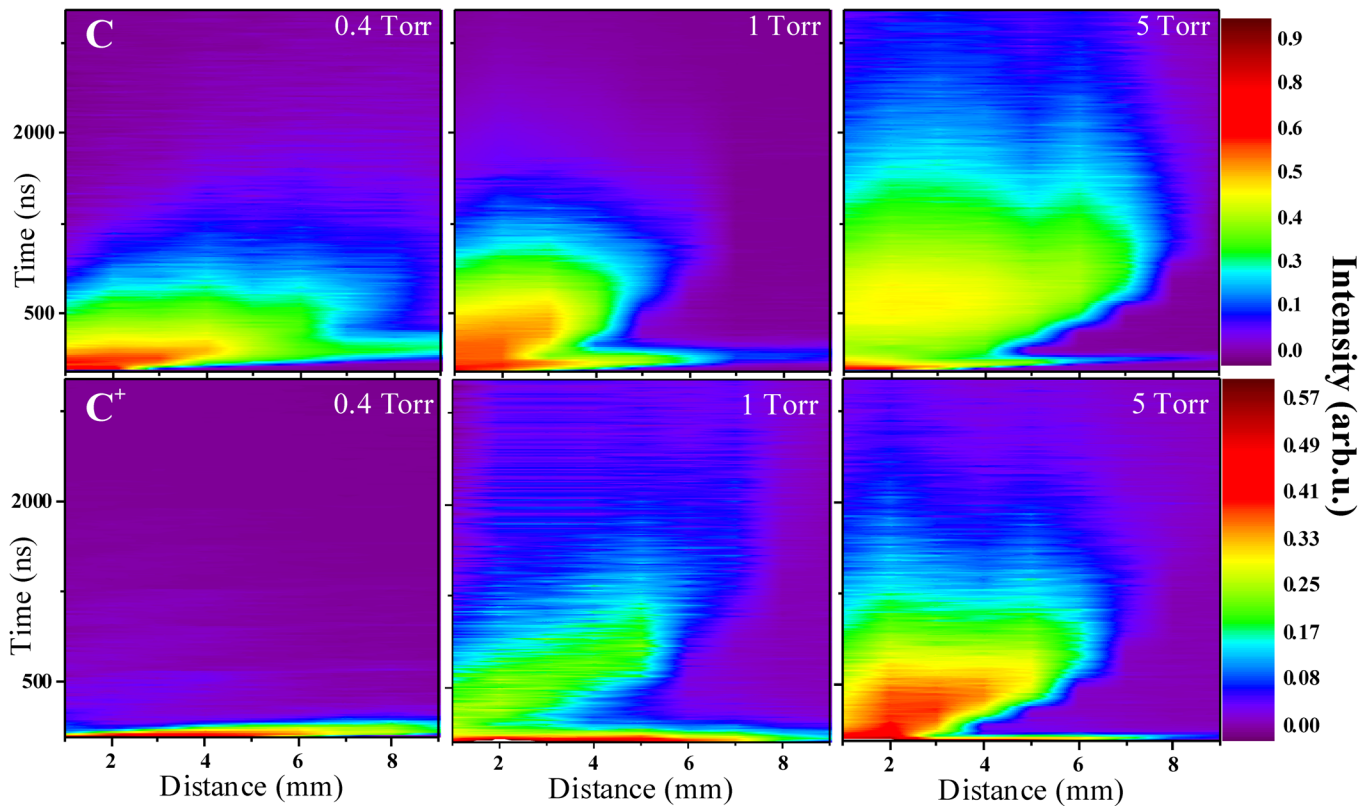
FIG. 12. Space-time contours for excited C ($\lambda = 247.8$ nm) and C^+ ($\lambda = 426.7$ nm) emissions in carbon fs LPP expanding at different helium pressures.

Moreover, fast imaging showed that plasma plume and C_2 emission was brighter and more confined in ambient nitrogen rather than in helium gas. The hydrodynamic features of ultrafast LA in the presence of moderate helium pressures were described well by the drag and adiabatic expansion models.

The spectral details obtained from ultrafast LA plumes showed predominant emission from neutral species as well as carbon dimers while ns LA showed significant emission from carbon lower-charged ions along with neutrals and dimers. In agreement with the monochromatic ICCD imaging, the OES

captures confirmed that C_2 is more intense but confined to closer zones using nitrogen as background gas in comparison with helium. C_2 vibrational temperatures were estimated and were found to decrease with distance and increasing ambient gas pressure. Due its high thermal conductivity and low mass, helium was more efficient than nitrogen gas for cooling plasma temperature. Along with fast imaging and OES of ultrafast LA of carbon plasma, OTOF-ES profiles were also generated for different excited (neutral and ionic) carbon species in addition to C_2 emitting zones. These measurements are extremely useful for tracking evolution of certain species during the plume expansion because of their high temporal resolution and high spectral purity. These profiles indicate that C and C^+ were presented by a double-peak structure while C_2 showed a unimodal temporal profile. The spatio-temporal contours show that C_2 emission intensity was found to peak at certain helium pressure (1 Torr) and then was confined at higher pressure (5 Torr). Connecting the results produced by the ICCD images, OES, and the spatio-temporal contours indicates that three-body recombination is a major mechanism for the generation of carbon dimers in ultrafast laser ablation plumes in the presence of an ambient gas. Integrating these multiple diagnostic methods in the present work helped in obtaining comprehensive vision of the history of various plume species development in ultrafast laser ablation plumes.
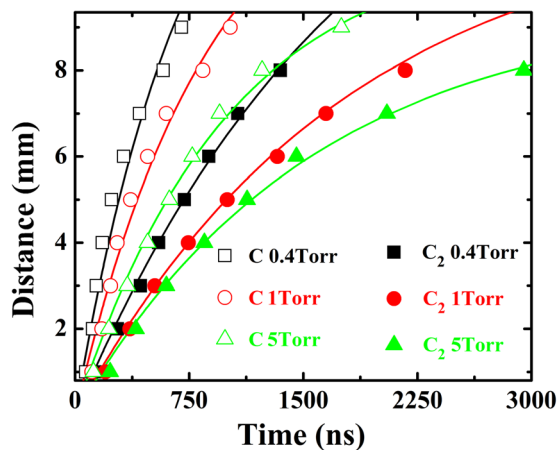

FIG. 13. Position–time (R-t) plots for C and C_2 emissions from fs carbon plasma expanding in ambient helium at varied pressures obtained from OTOF-ES measurements. The symbols represent experimental data points and solid curves represent the drag expansion model.

ACKNOWLEDGMENTS

[1]O. Albert, S. Roger, Y. Glinec, J. C. Loulergue, J. Etchepare, C. Boulmer-Leborgne, J. Perriere, and E. Millon, Appl. Phys. A **76**, 319 (2003).

[2]R. E. Russo, X. L. Mao, J. J. Gonzalez, and S. S. Mao, J. Anal. At. Spectrom. **17**, 1072 (2002).

[3]M. Q. Ye and C. P. Grigoropoulos, J. Appl. Phys. **89**, 5183 (2001).

[4]H. Dachraoui and W. Husinsky, Appl. Phys. Lett. **89**, 104102 (2006).

[5]B. Liu, Z. D. Hu, Y. Che, Y. B. Chen, and X. Q. Pan, Appl. Phys. Lett. **90**, 044103 (2007).

[6]F. Beffa, H. Jackel, M. Achtenhagen, C. Harder, and D. Erni, Appl. Phys. Lett. **77**, 2301 (2000).

[7]D. Grojo, J. Hermann, and A. Perrone, J. Appl. Phys. **97**, 063306 (2005).

[8]R. Stoian, D. Ashkenasi, A. Rosenfeld, and E. E. B. Campbell, Phys. Rev. B **62**, 13167 (2000).

[9]D. Bauerle, *Laser Processing and Chemistry* (Springer-Verlag, Berlin, 2011).

[10]B. Verhoff, S. S. Harilal, J. R. Freeman, P. K. Diwakar, and A. Hassanein, J. Appl. Phys. **112**, 093303 (2012).

[11]S. S. Harilal, A. Hassanein, and M. Polek, J. Appl. Phys. **110**, 053301 (2011).

[12]A. C. Dillon, P. A. Parilla, J. L. Alleman, J. D. Perkins, and M. J. Heben, Chem. Phys. Lett. **316**, 13 (2000).

[13]F. Qian, R. K. Singh, S. K. Dutta, and P. P. Pronko, Appl. Phys. Lett. **67**, 3120 (1995).

[14]M. K. Moodley and N. J. Coville, Chem. Phys. Lett. **498**, 140 (2010).

[15]J. J. Camacho, L. Diaz, M. Santos, D. Reyman, and J. M. L. Poyato, J. Phys. D: Appl. Phys. **41**, 105201 (2008).

[16]E. Cappelli, C. Scilletta, G. Mattei, V. Valentini, S. Orlando, and M. Servidori, Appl. Phys. A **93**, 751 (2008).

[17]F. Claeyssens, M. N. R. Ashfold, E. Sofoulakis, C. G. Ristoscu, D. Anglos, and C. Fotakis, J. Appl. Phys. **91**, 6162 (2002).

[18]F. Qian, V. Craciun, R. K. Singh, S. D. Dutta, and P. P. Pronko, J. Appl. Phys. **86**, 2281 (1999).

[19]S. Amoruso, G. Ausanio, R. Bruzzese, M. Vitiello, and X. Wang, Phys. Rev. B **71**, 033406 (2005).

[20]A. Van Orden and R. J. Saykally, Chem. Rev. **98**, 2313 (1998).

[21]K. F. Al-Shboul, S. S. Harilal, and A. Hassanein, Appl. Phys. Lett. **99**, 131506 (2011).

[22]K. F. Al-Shboul, S. S. Harilal, A. Hassanein, and M. Polek, J. Appl. Phys. **109**, 053302 (2011).

[23]R. W. Coons, S. S. Harilal, S. M. Hassan, and A. Hassanein, Appl. Phys. B **107**, 873 (2012).

[24]S. S. Harilal, R. W. Coons, P. Hough, and A. Hassanein, Appl. Phys. Lett. **95**, 221501 (2009).

[25]I. Labazan, N. Krstulovic, and S. Milosevic, J. Phys. D: Appl. Phys. **36**, 2465 (2003).

[26]Y. Iida and E. S. Yeung, Appl. Spectrosc. **48**, 945 (1994).

[27]S. Acquaviva and M. L. De Giorgi, Appl. Surf. Sci. **197–198**, 21 (2002).

[28]D. J. Hwang, H. Jeon, C. P. Grigoropoulos, J. Yoo, and R. E. Russo, Appl. Phys. Lett. **91**, 251118 (2007).

[29]K. F. Al-Shboul, S. S. Harilal, and A. Hassanein, Appl. Phys. Lett. **100**, 221106 (2012).

[30]A. A. Voevodin, J. G. Jones, J. S. Zabinski, and L. Hultman, J. Appl. Phys. **92**, 724 (2002).

[31]A. K. Sharma and R. K. Thareja, Appl. Surf. Sci. **243**, 68 (2005).

[32]D. B. Geohegan, Appl. Phys. Lett. **60**, 2732 (1992).

[33]C. S. Ake, R. S. de Castro, H. Sobral, and M. Villagran-Muniz, J. Appl. Phys. **100**, 053305 (2006).

[34]P. E. Dyer, A. Issa, and P. H. Key, Appl. Surf. Sci. **46**, 89 (1990).

[35]D. B. Geohegan, *Pulsed Laser Deposition of Thin Films* (Wiley, New York, 1994).

[36]S. Abdelli-Messaci, T. Kerdja, A. Bendib, and S. Malek, J. Phys. D: Appl. Phys. **35**, 2772 (2002).

[37]G. M. Fuge, M. N. R. Ashfold, and S. J. Henley, J. Appl. Phys. **99**, 014309 (2006).

[38]R. W. B. Pearse and A. G. Gaydon, *The Identification of Molecular Spectra* (Chapman and Hall, London, 1965).

[39]W. Weltner and R. J. Vanzee, Chem. Rev. **89**, 1713 (1989).

[40]Y. Yamagata, A. Sharma, J. Narayan, R. M. Mayo, J. W. Newman, and K. Ebihara, J. Appl. Phys. **86**, 4154 (1999).

[41]S. George, A. Kumar, R. K. Singh, and V. P. N. Nampoori, Appl. Phys. A **98**, 901 (2010).

[42]W. J. Liu, X. J. Guo, C. L. Chang, and J. H. Lu, Thin Solid Films **517**, 4229 (2009).

[43]L. Jiang and H. Tsai, in *Femtosecond Laser Ablation: Challenges and Opportunities* (Stillwater, OK, 2003), p. 163.

[44]J. R. Freeman, S. S. Harilal, P. K. Diwakar, B. Verhoff, and A. Hassanein, "Comparison of optical emission from nanosecond and femtosecond laser ablated brass plasma in atmosphere and vacuum," Spectrochim. Acta B (in press).

[45]A. Chehrghani and M. J. Torkamany, Opt. Lasers Eng. **51**, 61 (2013).

[46]G. Herzberg, *Spectra of Diatomic Molecules (Molecular Spectra and Molecular Structure)* (Van Nostrand, New York, 1950).

[47]W. Demtroder, *Atoms, Molecules and Photons: An Introduction to Atomic, Molecular and Quantum Physics* (Springer, 2010).

[48]E. Vors, C. Gallou, and L. Salmon, Spectrochim. Acta Part B **63**, 1198 (2008).

[49]R. K. Dwivedi and R. K. Thareja, Surf. Coat. Technol. **73**, 170 (1995).

[50]G. Callies, H. Schittenhelm, P. Berger, and H. Hugel, Appl. Surf. Sci. **127**, 134 (1998).

[51]P. T. Rumsby and J. W. M. Paul, Plasma Phys. Control. Fusion **16**, 247 (1974).

[52]S. S. Harilal, C. V. Bindhu, V. P. N. Nampoori, and C. P. G. Vallabhan, Appl. Phys. Lett. **72**, 167 (1998).

[53]S. S. Harilal, B. O'Shay, Y. Tao, and M. S. Tillack, J. Appl. Phys. **99**, 083303 (2006).

[54]J. P. Zheng, Z. Q. Huang, D. T. Shaw, and H. S. Kwok, Appl. Phys. Lett. **54**, 280 (1989).

[55]S. S. Harilal, R. C. Issac, C. V. Bindhu, V. P. N. Nampoori, and C. P. G. Vallabhan, J. Phys. D: Appl. Phys. **30**, 1703 (1997).

[56]S. J. Henley, J. D. Carey, S. R. P. Silva, G. M. Fuge, M. N. R. Ashfold, and D. Anglos, Phys. Rev. B **72**, 205413 (2005).

[57]R. K. Thareja, R. K. Dwivedi, and K. Ebihara, Nucl. Instrum. Methods Phys. Res. Sec. B **192**, 301 (2002).

[58]S. Acquaviva and M. L. De Giorgi, Appl. Surf. Sci. **186**, 329 (2002).

[59]A. Kumar, R. K. Singh, K. P. Subramanian, B. G. Patel, S. Sunil, and I. A. Prajapati, J. Phys. D: Appl. Phys. **39**, 4860 (2006).

[60]Z. Zelinger, M. Novotny, J. Bulir, J. Lancok, and M. Jelinek, Contrib. Plasma Phys. **44**, 360 (2004).